TU Delft

Delft University of Technology

Numerical investigation on particle swelling in spray roasting reactors

Schiemann, M.; de Haan, André; Wirtz, S.

DOI
10.1016/j.ijmultiphaseflow.2016.04.016

Publication date
2016

Document Version
Proof

Published in
International Journal of Multiphase Flow

Citation (APA)
Schiemann, M., de Haan, A., & Wirtz, S. (2016). Numerical investigation on particle swelling in spray roasting reactors. *International Journal of Multiphase Flow*, *85*, 38-47. https://doi.org/10.1016/j.ijmultiphaseflow.2016.04.016

Important note
To cite this publication, please use the final published version (if applicable).
Please check the document version above.

Copyright
Other than for strictly personal use, it is not permitted to download, forward or distribute the text or part of it, without the consent of the author(s) and/or copyright holder(s), unless the work is under an open content license such as Creative Commons.

Takedown policy
Please contact us and provide details if you believe this document breaches copyrights.
We will remove access to the work immediately and investigate your claim.

This work is downloaded from Delft University of Technology.
For technical reasons the number of authors shown on this cover page is limited to a maximum of 10.

Accepted Manuscript

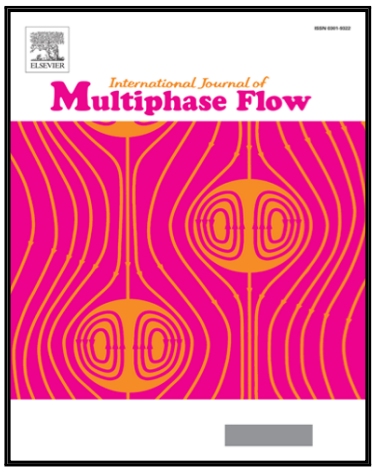

Numerical Investigation on Particle Swelling in Spray Roasting Reactors

M. Schiemann , A. de Haan , S. Wirtz

PII: S0301-9322(15)30135-X
DOI: 10.1016/j.ijmultiphaseflow.2016.04.016
Reference: IJMF 2385

To appear in: *International Journal of Multiphase Flow*

Received date: 5 November 2015
Accepted date: 20 April 2016

Please cite this article as: M. Schiemann , A. de Haan , S. Wirtz , Numerical Investigation on Particle Swelling in Spray Roasting Reactors, *International Journal of Multiphase Flow* (2016), doi: 10.1016/j.ijmultiphaseflow.2016.04.016

This is a PDF file of an unedited manuscript that has been accepted for publication. As a service to our customers we are providing this early version of the manuscript. The manuscript will undergo copyediting, typesetting, and review of the resulting proof before it is published in its final form. Please note that during the production process errors may be discovered which could affect the content, and all legal disclaimers that apply to the journal pertain.

ACCEPTED MANUSCRIPT

Highlights

- Spray roasting is a proven technique for metal chloride treatment.
- Particle swelling is a significant step in particle formation during spray roasting.
- Literature data was used to build particle swelling models for CFD simulations.
- The influence of particle swelling models is highlighted by the results.
- Recommendations for the use of numerical models and further experimental procedure are given.

ACCEPTED MANUSCRIPT

ACCEPTED MANUSCRIPT

NUMERICAL INVESTIGATION ON PARTICLE SWELLING IN SPRAY ROASTING REACTORS

M. Schiemann[1*], A. de Haan[2], S. Wirtz[1]

[1] *Department of Energy Plant Technology, Ruhr-University, Bochum, Germany*

[2] *Department of Chemical Engineering, Delft University of Technology, Delft, Netherlands*

**schiemann@leat.rub.de*

Abstract – Spray roasting of metal chloride solutions is frequently used to in steel industries to recover pickling liquids. As spray roasting reactors are difficult to characterize experimentally, computational fluid dynamics simulations have been used to investigate reactor performance. These simulations require a particle formation model, which describes the particles size history including the characteristic effect of particle swelling. Based on available literature, different swelling models are compared by simulations of an industrial scale reactor. The influence of particle swelling is discussed. The results clearly indicate the necessity to investigate particle swelling, potential collision effects and fragmentation for sound simulation of spray roasting reactors.

Keywords: spray roasting; iron chloride; pyrohydrolysis; particle morphology

1. INTRODUCTION

Spray Roasting reactors are useful tools to convert metal chloride or metal sulphide solutions to metal oxides and recover the chlorine or sulphur content (Peek, 1996). An example is the regeneration of iron chloride solutions in steel industries. Steel surfaces are pickled with aqueous hydrogen chloride to remove oxide layers from the surface. During this process, HCl is consumed forming $FeCl_2$ and small amounts of $FeCl_3$ in the solution, which leads to reduced

pickling ability. Instead of dumping the spent pickling liquid, thermal regeneration is a feasible technique to recycle HCl and to produce iron oxides as valuable by-product (Kladnig, 2003).

The global chemical reaction in this process is

$$4FeCl_2 + 4H_2O + O_2 \rightarrow 2Fe_2O_3 + 8HCl - 55{,}0\ kJ / mol_{Fe}.$$

Equation 1

Although the reaction is slightly exothermal, the typical water content of about 70%$_{mass}$ of water in the solution requires additional heat input, which is typically provided by natural gas combustion. To improve the process efficiency and to shorten evaporation and chemical conversion times, the solution is sprayed into the reactor, forming solid iron oxide particles from the solution.

The sprayed droplets undergo a multi-step conversion process in the spray roasting reactor (Beck et al., 2007b). The process starts with the evaporation of water (T= 373 K). During this process, the iron chloride concentration increases at the droplet surface, until the surface becomes impermeable for water vapor, causing increasing pressure which leads to swelling of the particle, producing particles with a diameter larger than the initial droplet diameter. When all water has been evaporated (note, that due to the tendency of iron chloride to form hydrates, part of the water evaporates at temperatures up to 538 K), the chemical conversion process starts.

Typical industrial scale spray roasting reactors are relatively large (more than 10 m high and 5 m in diameter) and work at high operating temperatures (~1000 K) (Beck et al., 2007b; Johansson et al., 2010; Schiemann et al., 2013; Westerberg et al., 2011). Additionally, the atmosphere inside these reactors contains large fractions of HCl, the flow field is turbulent and the droplet size distribution of the sprayed HCl solution is relatively wide (Beck et al., 2007b; Schiemann et al., 2015, 2013). These conditions render a detailed experimental analysis in industrial scale reactors difficult when the characterization of the iron oxide particles is of interest. Measurements which address the gas phase properties are possible under these

ACCEPTED MANUSCRIPT

turbulent conditions, e.g. gas temperature profiles as presented in (Johansson et al., 2010). Additionally, the plant roasting performance by detailed analysis of iron oxide samples produced under different operational parameters extracted at the particle outlet has been determined experimentally (Ferreira and Mansur, 2011). For deeper insight, numerical studies, namely computational fluid dynamics (CFD) simulations were used to investigate the effect of geometric variations in reactor design (Johansson et al., 2014; Westerberg et al., 2011).

When the particle formation and reaction process is of deeper interest, lab-scale experiments become important. Beck et al. investigated the formation of iron oxide particles in a small scale reactor with mono-disperse droplets (Beck et al., 2007a) in the diameter range of 100 µm, which led to a numerical particle formation model used in CFD simulations of a large scale reactor (Beck et al., 2007b). This model was expanded by Schiemann et al., who also carried out experimental work on 100 µm droplets (Schiemann et al., 2012) to augment the insight into the particle formation process. Their model was the first to include particle swelling, which leads to the characteristic formation of particles shaped as hollow spheres. This model was used for CFD simulations of industrial scale spray roasters (Schiemann et al., 2013).

As the previous experimental work focused on particles in the size range of 100 µm (Beck et al., 2007a; Schiemann et al., 2012), but the prevailing particle size distribution in iron chloride spray roasting extends from a few µm to nearly one mm (Schiemann et al., 2013), a new experimental approach was used to investigate the particle formation process for droplets in the upper size limit. The experiments for the investigation of smaller particles were carried out using drop tube reactors with falling droplets/particles, but the drying time for droplets at the upper size limit exceeds the residence time in drop tube reactors. Therefore, droplets of approx. 1 mm diameter were dried by laser heating in an acoustic levitator (Schiemann et al., 2015). These experiments added information on the formation of cenospheres from larger droplets of iron chloride solution. It was shown, that the particle diameter decreased in these experiments, but was still larger than a resulting solid spherical particle would have been, indicating minor but still relevant swelling.

Based on the experimental findings in (Schiemann et al., 2015, 2012), this paper evaluates the influence of particle swelling modelling on CFD simulations of a typical spray roaster. Three different mathematical models to fit the droplet/particle diameter correlation are used to compare the influence of different assumptions for particle swelling. As the results show, current literature data provide a fundamental base for reactor modelling, but the sensitivity of reactor simulations on particle swelling demands to handle this effect with care.

2. SET-UP

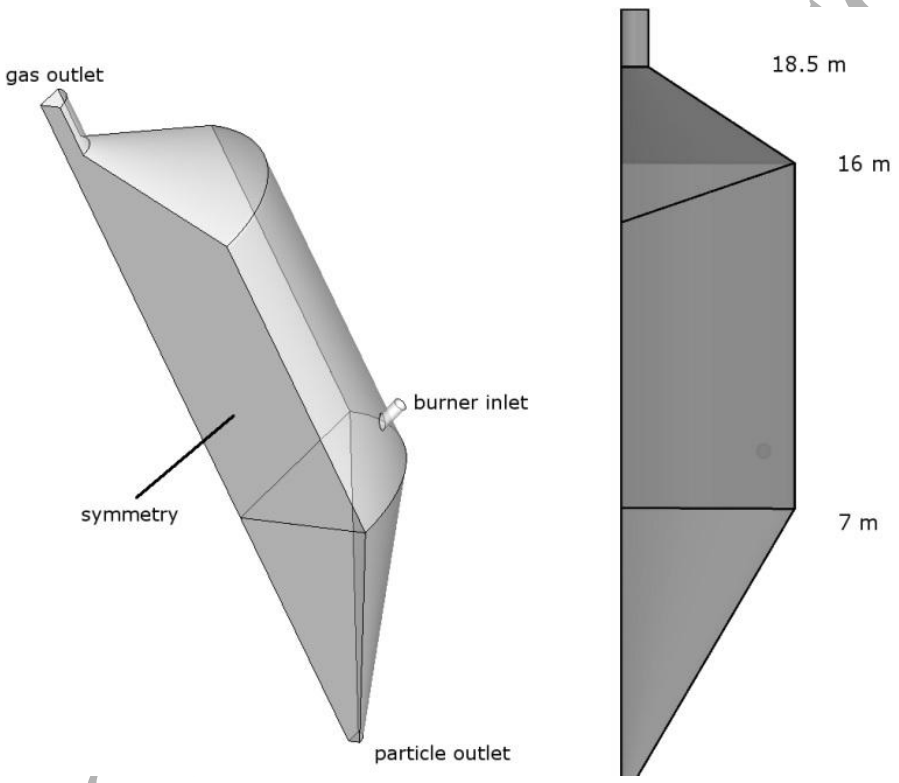

Figure 1: Schematic drawing of the reactor, represented by a quarter domain. The tangentially mounted burner is only partially simulated. The nozzle head is in the upper third of the reactor.

A generic geometry of a typical industrial iron chloride spray roaster has been developed according to (Johansson et al., 2014), a quarter section of the reactor is depicted in Figure 1. The total height of the considered domain is 20 m with a diameter of 9 m. The diameters of gas and particle outlet are 1.4 m and 1 m respectively. The burner, which is only partially simulated to

keep the gas combustion model simple for acceptable computation times, has a diameter of 0.3 m. The computational domain was limited to one quarter of the total reactor using a symmetric design to reduce the computational effort. Of course, using symmetry conditions can have measurable effects on calculated flow field, but compared to results of previous simulations of spray roasters (Beck et al., 2007b; Schiemann et al., 2013) without symmetric boundary conditions no significant differences were found, which justifies the approach. A hexagonal mesh with 220.000 cells was used, and mesh dependency effects were found to be negligible for the questions which are investigated in the current work.

The energy demand of the process is in the order of 2.9 $MJ/l_{solution}$ and slightly varies with plant size and $FeCl_2$ concentration in the liquid feed (Jedlicka, 1978). The natural gas feed was substituted by a partially reacted methane-air mixture with mass flow, composition and temperature given in Table 1, as the complete simulation of the burner tube requires very high computational effort and is not the major purpose of this work. The conditions (mass flow, temperature) were chosen based on the energy demand and the fact that the gas typically reacts partially in the burner tube, but complete reaction should take place in the reactor chamber, as the brick lining at the burner entrance to the reactor is limited to temperatures of 1300 K_{max}. The iron chloride solution was injected at a height of 14.5 m and a radial distance of 1.7 m from the centre axis. 0.4 $kg_{solution}/s$ with a $FeCl_2$ concentration of 30%$_w$ of iron chloride were injected with a particle size distribution $Y = 1 - exp(-d/300)^{2.48}$ (Schiemann et al., 2013), where Y denotes the cumulative particle mass below d, which is the particle diameter in µm. The nozzles (typically around 10-15 placed on a circular holder) were not resolved in the simulation. However, the injection of 1600 particles was simulated, subdivided into 20 size fractions in the range 100-450 µm, as solid cone with an initial $v_{droplet}$= 10 m/s and a cone angle of 45° directed downwards. The injections were spread over a surface of 20 cm diameter to approximate the effect of the nozzle holder.

3. MODELING APPROACH

The simulations were carried out using the commercial CFD code Ansys Fluent 15. The general proceeding is similar to the work described in (Schiemann et al., 2013, 2012), so only a brief description is given here.

An incompressible flow was simulated using the Reynolds averaged Navier-Stokes (RANS) approach, solving the continuity and momentum equations in Reynolds-averaged simulations:

$$\frac{\partial}{\partial x_i}(\overline{\rho u_i}) = 0 \qquad \textbf{Equation 2}$$

$$\frac{\partial}{\partial x_i}(\overline{\rho u_i u_j}) = -\frac{\partial \bar{p}}{\partial x_i} + \frac{\partial}{\partial x_j}\left[\mu\left(\frac{\partial \bar{u}_i}{\partial x_j} + \frac{\partial \bar{u}_j}{\partial x_i} - \frac{2}{3}\delta_{ij}\frac{\partial \bar{u}_l}{\partial x_l}\right)\right] + \frac{\partial}{\partial x_j}\left(-\rho\overline{u_i' u_j'}\right). \qquad \textbf{Equation 3}$$

where ρ denotes the gas density in a cell, t and x denote time and spatial direction (indices mark single components) and u is the velocity. μ is the turbulent viscosity. The simulations were carried out using second order upwind discretisation and pressure-velocity coupling using the SIMPLE scheme, while the PRESTO! mechanism was used for pressure.

Turbulence modelling was carried out using the k-ω-SST model (Menter, 1994), which was found to provide the best ability to consider the wall effects in the rotating gas flow typical for spray roasters (Schiemann et al., 2013). It is represented by the governing equations for the turbulent kinetic energy k and the specific dissipation rate ω:

$$\frac{\partial}{\partial x_i}(\rho k \bar{u}_i) = \frac{\partial}{\partial x_j}\left(\Gamma_k \frac{\partial k}{\partial x_j}\right) + \tilde{G}_k - Y_k + S_k \qquad \textbf{Equation 4}$$

$$\frac{\partial}{\partial x_i}(\rho \omega \bar{u}_i) = \frac{\partial}{\partial x_j}\left(\Gamma_\omega \frac{\partial \omega}{\partial x_j}\right) + G_\omega - Y_\omega + D_\omega + S_\omega. \qquad \textbf{Equation 5}$$

Note, that $\tilde{G}_k$represents the generation of turbulent kinetic energy by mean velocity gradients, G_ω denotes the generation of ω, and the effective diffusivity and dissipation of k and ω are given by Γ and Y, respectively. User-defined source terms are included by $S_{k/\omega}$. By default, the k-ω-SST

ACCEPTED MANUSCRIPT

model as implemented in FLUENT uses enhanced wall treatment, which reduces the sensitivity to y^+ thus that $y^+ < 300$ becomes acceptable.

The burners are only partially included in the simulation. A detailed burner simulation requires precise knowledge of the burner geometry, exact determination of the feed gas composition (literature mentions coke oven gas, natural gas and light oil (De Bakker, 2011; Kladnig, 2008)) and usually requires high numerical effort in terms of meshes with high spatial resolution and detailed combustion models. However, this work focusses on the particle formation process and not on the influence of burner details. Therefore a simplified representation of the combustion reaction in the burner was chosen, and the burner geometry was not fully included in the geometry (Figure 1). Gas phase combustion was modelled using the eddy dissipation model (Magnussen and Hjertager, 1977), which was applied to solve the methane-air 2-step mechanism developed by Westbrook and Dryer (Westbrook and Dryer, 1981). A more detailed description on their working principle and implementation can be found in (Ansys, 2011). It is obvious that this simplified model cannot handle the complex reaction schemes appearing in a turbulent NG flame. However, it provides a suitable flame structure with the final burnout taking place in front of the burner, which is important to keep the momentum transfer in the right range.

Radiation modelling was carried out using the discrete ordinates approach (Raithby and Chui, 1990) and the weighted-sum-of-gray-gases model to consider gas radiation effects (Smith et al., 1982).

The dispersed phase was modelled using the Lagrangian approach, updating the source terms of the continuous phase every ten iterations, which itself is based on the Eularian approach. Before the phenomena which are considered in the particle model are explained, a brief summary is given on the steps each particle experiences:

- After being injected, a droplet is inertially heated up to the boiling temperature (373 K) of water.

ACCEPTED MANUSCRIPT

- When the boiling temperature is reached, water begins to evaporate.
- The mass loss from evaporation leads to the formation of a concentration gradient of iron chloride, which is accumulated at the droplet surface.
- The accumulation of iron chloride at the surface leads to formation of a solid shell, which causes the formation of cenospheric particles and particle swelling, as the particle is not completely dry at this point. Remaining water vapour is trapped inside the shell and temperature increase causes a pressure increase and thus particle swelling (Beck et al., 2007a).
- The particle contains significant amounts of water at the beginning of the swelling process, consisting of $FeCl_2 \cdot 4H_2O$ and some excess water. The swelling process continues until all water is evaporated and the particle solely consists of $FeCl_2$.
- When the particle has reached this point, the chemical conversion process starts and Fe_2O_3 is formed, which causes a mass increase while the particle diameter remains constant.

Before the swelling model, which is the object of major interest of the current work, is discussed in detail, the general droplet/particle model is described briefly. All sub models which describe the discrete phase are implemented in a user-defined function, which considers all changes of the subject (diameter, density, chemistry) and connects these properties to the equations to calculate particle movement, heat and mass exchange.

Particle motion was calculated from the sum of buoyancy and drag, leading to

$$F_p = (m_p - m_f)g + \frac{1}{2} C_D \rho_f A_f |v_f - v_p| (v_f - v_p), \qquad \textbf{Equation 6}$$

where the index p denotes particle related variables und f marks fluid properties. m is the mass of given components, g is the apparent gravity, C_D is the drag coefficient, A_f the cross sectional area of the particle and v denotes velocities. Particle or droplet collisions were not considered. Particle trajectories were resolved to time steps smaller than 1 ms.

The evaporation of water below the boiling point is neglected, as the time span which a particle spends in this regime is rather short, as is shown later in Figure 6, and the corresponding amount of water evaporating is assumed to be rather small. When a droplet of iron chloride solution reaches the boiling point of water (T_p= 373 K), the mass loss is calculated by

$$\frac{d(d_p)}{dt} = \frac{2}{\rho_p h_{fg}}\left[\frac{\lambda\, Nu}{d_p}(T_\infty - T_p) + \varepsilon_p \sigma(\theta_R^4 - T_p^4)\right]. \qquad \textbf{Equation 7}$$

The quantities included are the droplets density ρ_p, its diameter d_p and temperature T_p, the thermal conductivity of the surrounding gas phase λ, and the latent heat of water h_{fg}. The Nusselt number is calculated using the correlation $Nu = 2 + 0.6\sqrt{\mathrm{Re}}\sqrt[3]{\mathrm{Pr}}$. It has to be noted, that the release of water is not completed in one step at the standard boiling point of water, but part of the water is supposed to be chemically bound to the iron chloride forming $FeCl_2 \cdot 4H_2O$, which loses two molecules of water at T= 379 K, a third molecule at T= 433 K and becomes dry $FeCl_2$ at T= 538 K (Schiemann et al., 2013, 2012). The evaporation of the bound water is calculated based on the energy input which is required to split the bonds between the water molecule and the residual molecule. The conversion from $FeCl_2 \cdot 4H_2O$ to $FeCl_2$ requires approx. 5 kJ/g_{Fe} which is half of the energy necessary for evaporating the excess water in advance. Between the different drying stages the particle is inertly heated.

The chemical conversion has been split in to two sub-reactions, splitting of HCl by the reaction

$$4FeCl_2 + 4H_2O \rightarrow 4FeO + 8HCl - 508kJ/mol \qquad \textbf{Equation 8}$$

followed by the complete oxidation in the reaction

$$4FeO + O_2 \rightarrow 2Fe_2O_3 + 563kJ/mol\,. \qquad \textbf{Equation 9}$$

Both reactions have been investigated for the influence of chemical kinetics, pore diffusion and boundary diffusion of the gaseous reactants H_2O and O_2 (Schiemann et al., 2012). As the dominating pore size was found to be in the range of 4-5 nm, pore diffusion was identified as leading effect for the determination of the reaction rate.

Source terms are used to couple the mass, heat and momentum exchange between discrete and continuous phase.

3.1 Particle Swelling

The most important part in the present work is the effect of particle swelling. The formation of particles in the shape of hollow spheres has been found in experimental work carried out in lab-scale drop tube reactor experiments (Beck et al., 2007a; Schiemann et al., 2012), by laser heating of levitated particles (Schiemann et al., 2015) and in large scale spray roasters (Ferreira and Mansur, 2011).

With beginning evaporation the chemical composition of the particle changes. As there is no known model describing the density of a water/iron chloride/iron oxide mixture, the density is calculated based on a mass-weighted approach as

$$\rho_p = \frac{1}{m_p}\left(\sum_i m_i \rho_i\right) \qquad \textbf{Equation 10}$$

This equation, including the particle mass m_p, m_i as the mass of the i-th component (considered are unbound water, water bound to iron chloride tetra hydrate, pure iron chloride, FeO (wustite) and Fe_2O_3 (hematite)) and ρ_i as corresponding density, is used for the complete chemical conversion process.

The evaporation process leads to an enrichment of iron chloride on the droplet surface. When the iron chloride concentration at the particle surface reaches a critical concentration, the droplet surface becomes impermeable for water vapour, which leads to an increase in pressure and as a result the particle starts swelling.

In previous work (Beck et al., 2007a; Schiemann et al., 2012), a model first published by Brenn (Brenn, 2004) was used to calculate the concentration gradient of iron chloride and thus the critical concentration in the boundary layer which determines the starting point of the swelling

process. The mass fraction $Y(\tau,\xi)$ of the remaining substance ($FeCl_2$) is calculated by the following equation:

$$Y(\tau,\xi) = \sum_j C_j(1+\alpha\tau)^{-\lambda_j} \cdot M_K\left(\lambda_j, \frac{3}{2}, -\frac{\alpha}{4G}\xi^2\right) \quad \textbf{Equation 11}$$

The parameters needed to calculate the critical mass fraction are dimensionless time τ, diameter ξ, shrinking rate α and diffusion coefficient G, as well as the specific eigenvalues of the problem λ_j. Additionally the Kummer function M_K is needed (Abramowitz and Stegun, 1972). The shrinking rate is a parameter of certain importance. It depends on the drying conditions, i.e. heat flux to the particle and evaporation rate.

Previously it was assumed that the critical concentration is reached when the outer shell of the particle consists of 64%$_w$ of $FeCl_2$, corresponding to pure $FeCl_2{\cdot}4H_2O$. The increasing pressure in the particle now leads to an increase in diameter, calculated as

$$d_p(m_p) = d_0\left[1 + \frac{d_f}{d_0}\frac{1}{1-\bar{Y}_{FeCl_2}}\frac{m_{p,0}-m_p}{m_{p,0}}\right] \quad \textbf{Equation 12}$$

This equation includes the initial droplet diameter d_0, the average $FeCl_2$ concentration $\bar{Y}_{FeCl2}$ calculated by integrating Equation 11 depending on the initial droplet size, the particle mass $m_{p,0}$ at the starting point of the swelling process and the actual particle mass m_p. The swelling process stops when the particle has reached the mass of pure $FeCl_2$, thus it is completely dry. As the particle mass is not affected by swelling, but the particle forms the typical cenospheric structure, the diameter of the internal void is calculated as

$$d_i = \sqrt[3]{d_p^3 - \frac{6}{\pi}\frac{m_p}{\rho_p}}. \quad \textbf{Equation 13}$$

The particle diameter d_p is calculated using Equation 12, while ρ_p follows from Equation 10, thus the particle mass is concentrated in the shell of the particle.

The final particle diameter d_f has been in the focus of experimental investigations of iron chloride spray drying. Drop tube experiments with single droplets with diameters of 66 µm and 89 µm initial droplet diameter were presented in (Schiemann et al., 2012). The experimental conditions were chosen to meet the average temperature of spray roasting reactors (~900 K). From these experimental results, a relation of initial droplet diameter and final particle diameter was elaborated, leading to a linear ratio between initial droplet and final particle diameter $d_f = 2.19 \cdot d_0$. Further experiments were carried out using levitated droplets in the mm size range (Schiemann et al., 2015) to cover the upper size limit of typical droplet size distributions (Schiemann et al., 2013). These results show a different tendency. Although the formation of hollow spheres during the drying process is reported, the resulting particle is smaller than the initial droplet ($d_f(d_0 = 1mm) = 612 \pm 160\mu m$). These different results are summarized in Figure 2.

As Figure 2 shows, the linear model overestimates the final diameter of levitated droplets clearly. This leads to the question, whether the assumption of a constant ratio between initial and final particle diameter, which was physically justified in (Schiemann et al., 2013, 2012), is suitable and how it affects the predicted performance of spray roasting reactors by CFD simulations. As a test, two empirical relations were employed to calculate d_f in dependence of d_p, one power law ($d_f = (2.1\pm0,1)*10^{-3} d_p^{(0.512\pm0,107)}$) and one logarithmic law ($d_f = (1.72\pm0,03)*10^{-4}\ln(d_p)+(1.8\pm0,1)*10^{-3}$). The error was calculated from the regression of the corresponding particle size relation using the standard deviations of 13, 22.1 and 160 µm for initial droplet sizes of 66, 89 and 1000 µm (Schiemann et al., 2015, 2012). Both relations were chosen as they are mathematically simple and can be fitted to the measured particle sizes. As Figure 2 shows,

they are quite similar in the considered particle size range. However, when the initial droplet

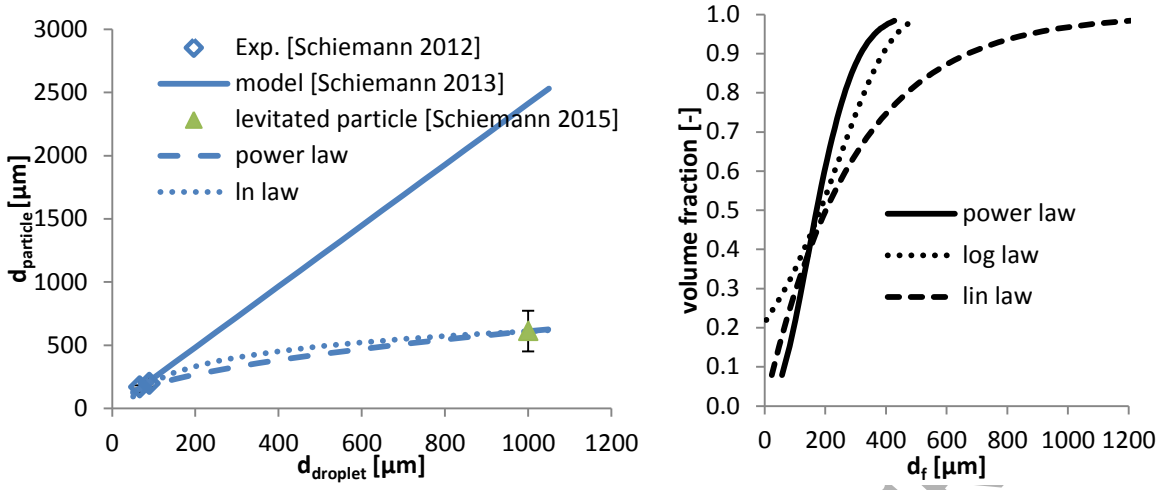

Figure 2: Left: Experimental droplet/particle size correlations from (Schiemann et al., 2012) **and** (Schiemann et al., 2015) **compared to the model published in** (Schiemann et al., 2013) **and to empirical correlations with the purpose to fit all experimental data. Right: Volumetric particle size distribution for resulting final diameter d_f.**

size distribution is considered to calculate the volumetric particle size distribution for the final particle diameter, a difference for both models becomes visible. While the power law and the linear law are relatively similar for d_f< 200 µm, the logarithmic law leads to a very high content of small particles. Compared to the linear model, both alternative approaches cover a smaller final particle size range. The consequence of these differences will be investigated in the following.

4. Numerical Results

All simulations were calculated until several convergence criteria were met. First, mass weighted temperature averaged at the gas outlet (top of the reactor) and in the whole domain, has to remain on the same level. Second, gas velocity magnitude, averaged in the same way, was monitored. Third, the residuals of all equations solved for the gas phase and radiation were expected to settle at constant level below 10^{-3}.

The linear model (Figure 2, (Schiemann et al., 2013)) was used as reference case, thus the gas phase properties resulting from the application of this model in CFD simulations are discussed

ACCEPTED MANUSCRIPT

by counter plots of different gas phase properties to characterize the general flow field of this spray roaster configuration.

In Figure 3, the symmetry plane is used to visualize the gas phase properties. The temperature is highest at the burner level in the near-wall region. The gas temperature in large parts of the centre region is slightly above 1000 K, with significant heat loss in the near wall region and close to the particle outlet. The hot spot in the middle near-wall region marks the burner gas inflow, where the gas temperature exceeds 1700 K. The water vapour concentration is highest on the level of the nozzle head, which is in agreement with the HCl concentration. While the water vapour mass fraction reaches nearly 20%, the HCl content is above 7.5% in this zone.

The tangential velocity, which characterizes the rotating flow field, peaks at the burner inflow and shows vertical layers with a strong velocity gradient from the wall to the reactor symmetry axis, where its value reduces to less than 2 m/s. The vertical velocity, which is important for the vertical particle movement, shows an upstream gas flow in the reactor centre line, while in the near wall region and between the burner and the centre, slightly negative velocities are found. The turbulent intensity is highest in the gas jet produced by the burner, and a zone of elevated turbulent intensity stretches from the burner upwards to the gas outlet.

ACCEPTED MANUSCRIPT

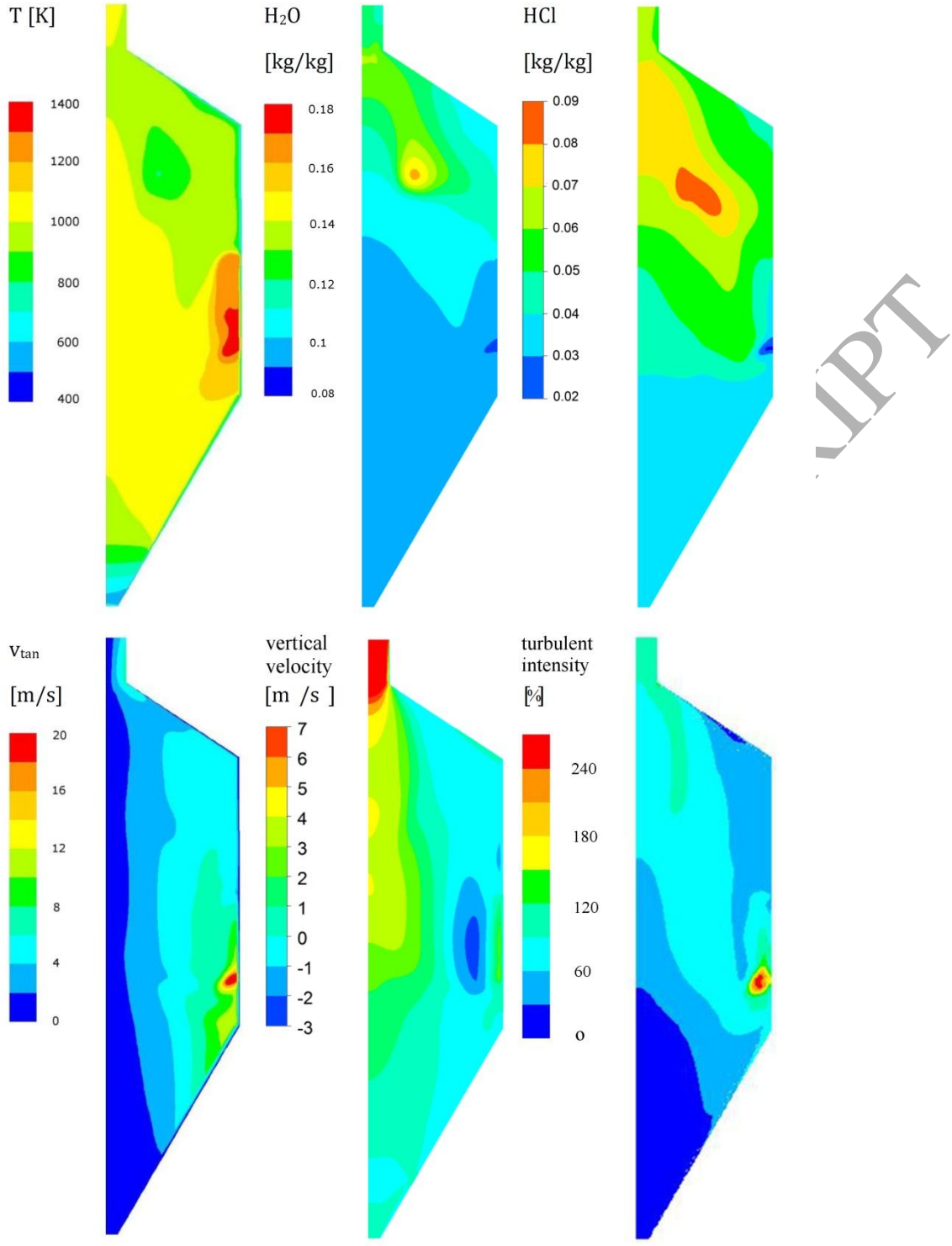

Figure 3: Counter plots of the symmetry plane using the linear particle swelling model, top row: temperature, water vapour mass fraction, HCl mass fraction, bottom row: tangential velocity v_{tan}, turbulent kinetic energy k and Reynolds number.

Application of the two alternative particle swelling models (power law and logarithmic model) leads to significant changes in the continuous phase, as is shown in Figure 4. Mass averaged gas phase properties were summarized by calculating the average $\bar{\varphi}(z) = \sum_i \left(\varphi_i(z) m_i(z)\right) / \sum_i m_i(z)$

for the measurands (φ) temperature, mass fraction (concentration) of HCl and water vapour, tangential velocity, turbulent kinetic energy and Reynolds number. Z denotes the sampling height, varied in steps of 1 m between 2 m and 18 m and m_i is the mass in cell i. Significant differences appear between the three swelling models. Compared to the linear model, the power law model leads to higher gas temperatures in the lower part of the reactor and lower temperatures with increasing height. The temperature profile resulting from the logarithmic swelling model shows a similar trend as the power law model, but the profile is shifted to slightly higher temperatures, being up to 100 K higher than the power law model close to the particle outlet. The concentration profiles of HCl (open symbols) and water vapour (closed symbols) also show clear differences. The HCl concentration at the topmost sampling position is slightly lower when the linear model is applied. The two alternative models show slightly higher but comparable HCl concentrations among themselves. Below the 14 m level larger differences appear. While the concentration is constant between 14 m and 8 m for both models, below an increase appears which is stronger for the power law model. The water vapour concentration also differs for the three models. At the reactor top linear and power law model are nearly on the same level, which is exceeded by the logarithmic model. The lower HCl and higher H_2O concentrations in the bottom section resulting from application of the linear model compared to the two alternatives indicates that the roasting reactions, which are exothermic in sum, take place in higher parts of the reactor when this model is applied. The heat release of particles which undergo the final reaction step in the lower reactor half misses in this case.

The logarithmic model has the highest H_2O concentrations, being approx. 0.02 kg/kg above the power law model, but the trend for both models is very comparable. The H_2O concentration resulting from linear particle swelling is lowest in the reactor middle, but shows a minor increase close to the particle outlet, where it nearly reaches the level of the logarithmic model.

The flow field variables also depict differences between the three models. The tangential velocity caused by linear particle swelling is slightly lower in the upper reactor half and slightly higher at 4-7 m compared to power law and ln model, which are on a comparable level. The turbulent

ACCEPTED MANUSCRIPT

kinetic energy is highest on burner level, resulting from the high momentum of the burner inflow. The linear model is lowest at this position, while it slightly exceeds the value of the two competing models at 14-16 m. The Reynolds number profiles show similar tendencies with peak values at 14 m and decreasing tendencies to the upper and lower reactor ends, but the Reynolds number of the linear model exceeds the other two cases up to 30%.

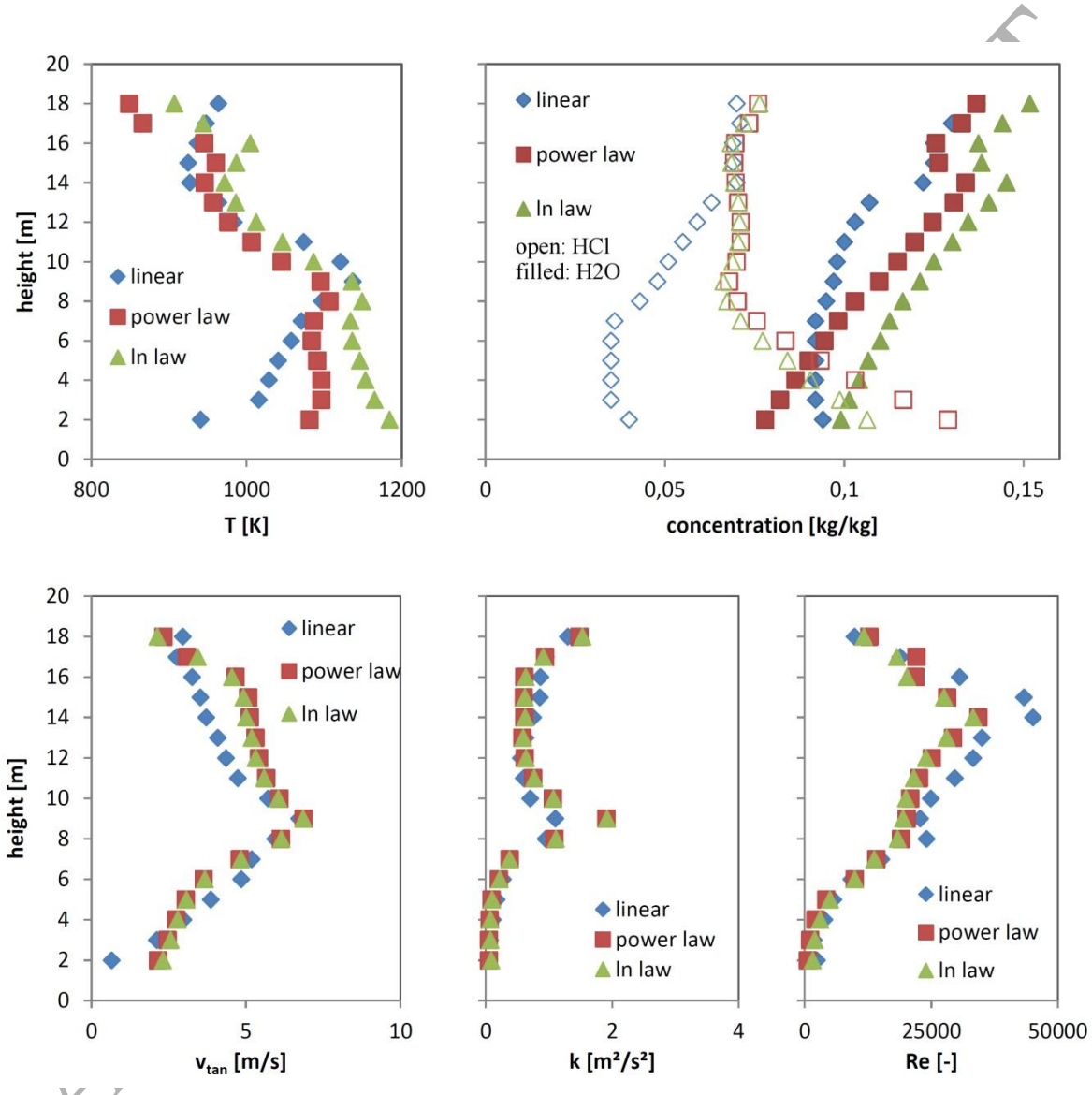

Figure 4: Mass averaged gas phase properties in horizontal sampling planes along the reactor height. Top right: HCl open symbols, H_2O filled symbols.

As the influence on the continuous phase is clearly visible, analysis of the discrete phase is necessary as particle quality is the major issue in spray roasting reactors. Typical particle properties are the conversion in terms of Cl_2 and FeO content, which determines the purity for subsequent use of the iron oxide.

The particle composition at the particle outlet is summarized in Table 2. All models lead to a particle composition which is acceptable for subsequent use of the particles in industrial applications, as the predicted chlorine content and FeO content are below 1 w%. In simulations using the linear swelling model very small impurities were found, and the particles consisted of 99.98 w% Fe_2O_3. Additionally, the average residence time of the particles in the reactor was calculated, and this shows that increasing residence time leads to decreasing impurities.

5. Discussion

The profiles of the gas phase and the particle samples at the particle outlet already show that the influence of the swelling model applied has a significant influence on the flow field, the local species concentration and the predicted chemical quality of the iron oxide particles. It is obvious that the final particle diameter given in Equation 12 defines the governing part of the particle motion and thus determines the local properties of the chemistry and the flow field. The investigated models in this work are based on final particle diameters gained from two different experiments. Droplets with initial sizes of less than 100 µm were investigated in a drop tube reactor, where these droplets were injected into atmospheres with a gas temperature of approx. 900 K (Schiemann et al., 2012). In these experiments, the final diameter was found to increase by a factor higher than 2 compared to the initial diameter. Droplets of 1 mm initial diameter were investigated in levitation experiments and heated with a CO_2 laser (Schiemann et al., 2015). The final particles extracted from these experiments finally showed a diameter of approx. 0.6 mm, which is shrinkage of 40%, but as in the previous experiments, the typical particle structure of hollow spheres was found.

In all models the beginning of the swelling process is determined using Equation 11 for the radial concentration of the solute (iron chloride) in the solvent (water). The concentration profile is integrated to calculate the average iron chloride content, which is tracked in the simulation. From the parameters which are used to calculate the radial iron chloride concentration, the shrinking rate α, which is closely related the drying history, is identified to be

ACCEPTED MANUSCRIPT

most sensitive to the boundary conditions which lead to droplet evaporation. The diffusion coefficient for iron chloride in water can be calculated to $5*10^{-12}$ m^2/s using the Wilke–Chang correlation (Wilke and Chang, 1955), and it is supposed that this value does not change significantly over a wide range of varying concentrations (Brenn, 2005). The dimensionless shrinking rate α is defined as

$$\alpha = \tilde{\alpha}\,\frac{t_l}{d_o^2}, \qquad \textbf{Equation 14}$$

with $\tilde{\alpha} = \frac{d d_p^2}{dt}$ and $t_l = \frac{d_0^2}{\tilde{\alpha}}\left[\left(\frac{\overline{Y_{20}}}{(1-\bar{Y}_{20})^{\rho_{s2}}/_{\rho_1}+\bar{Y}_{20}}\right)^{2/3} - 1\right]$ where $\bar{Y}_{20}$ is the initial concentration of the solute, ρ_{s2} and ρ_1 are the densities of solute and solvent respectively. It furthermore shows that $\tilde{\alpha}$ is assumed to follow a classical d_2-law, such that the change of the droplet surface occurs with constant velocity. However, for iron chloride particles, to the author's best knowledge, no experiments are known which prove this relation by direct measurement. Instead the only assessment of droplet shrinking rate for iron chloride particles has been carried out by simulating a laboratory experiment, connecting measured droplet (66 and 89 µm) and particle diameters with numerically determined shrinking rates (Schiemann, 2011; Schiemann et al., 2012). The models which were employed in those CFD simulations are exactly the same as applied to large scale simulations in the current work, thus the heat transfer causing the mass loss and determining the shrinking rate is calculated in the same way in both simulations. d_p^2 resulting from these simulations, which were carried out for a gas temperature around 900 K in a drop tube with relatively cold walls (T_w~ 400-500 K) is plotted in Figure 5. Additional trend lines describe the shrinking phase of the particles, which is well represented by $\tilde{\alpha}$= 33700 $\mu m^2/s$.

For the levitation experiments reported in (Schiemann et al., 2015), the time scale until the particle size kept constant during drying is reported to be in the range of 32 s for particles reducing their diameter from 1 mm to 640 µm. This is the fastest shrinking observed in these experiments. Calculating $\tilde{\alpha}$ as difference quotient from initial and final diameter divided by the

drying time results in $\tilde{\alpha}$= 18450 µm^2/s, half the shrinking rate given for the drop tube experiments, which causes a lower concentration gradient of $FeCl_2$, as water diffusing in the $FeCl_2$-rich shell reduces the inhomogeneity, and leads to the formation of smaller particles with a thicker and thus more stable shell.

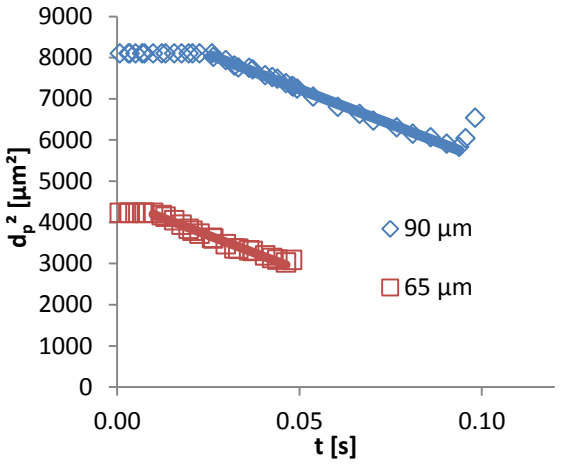

Figure 5: d_p^2-t relation taken from CFD simulations of particles in a drop tube reactor designed to match large scale reactor boundary conditions (Schiemann, 2011; Schiemann et al., 2012)**.**

The experimental data show a spread in shrinking rates approx. by a factor of two. Considering the suggested models for particle swelling and the numerical results corresponding to these, the shrinking rate of characteristic particles has to be compared to the experimental data. To represent the particle size distribution droplets with diameters of 80, 200 and 400 µm were investigated. As the spray cones in the industrial scale reactor lead to varying particle trajectories, 100 particles evenly distributed over the spray cone angle of 22.5° were sampled. For each of the particle diameters the particle trajectories were averaged in time steps of 3, 5 and 7.5 ms, respectively, with increasing particle size. As the time step size is related to the cell size and the particle velocity, the number of data points in each time step is not constant, thus it was averaged as $\bar{t}_{step} = \sum_{i=1}^{n} t_{i,step}/n$, and the diameter was calculated in accordance as $\bar{d}_{step} = \sum_{i=1}^{n} d_{i,step}/n$. The arithmetic mean value is plotted against time in Figure 6. As different particles experience different drying curves, for each of the time steps the minimum and maximum particle diameter were also depicted in Figure 6 to give an impression of the scatter of

the data. It has to be noted that the standard deviation, which one would expect instead of min/max values does not support the interpretation of the data. When a dominating fraction of the particles is not yet in the swelling phase, but some early particles already show increasing diameter, the standard deviation σ can become larger than the difference between minimum and average diameter, thus the difference $d_{mean} - \sigma$ becomes smaller than d_{min} and thus

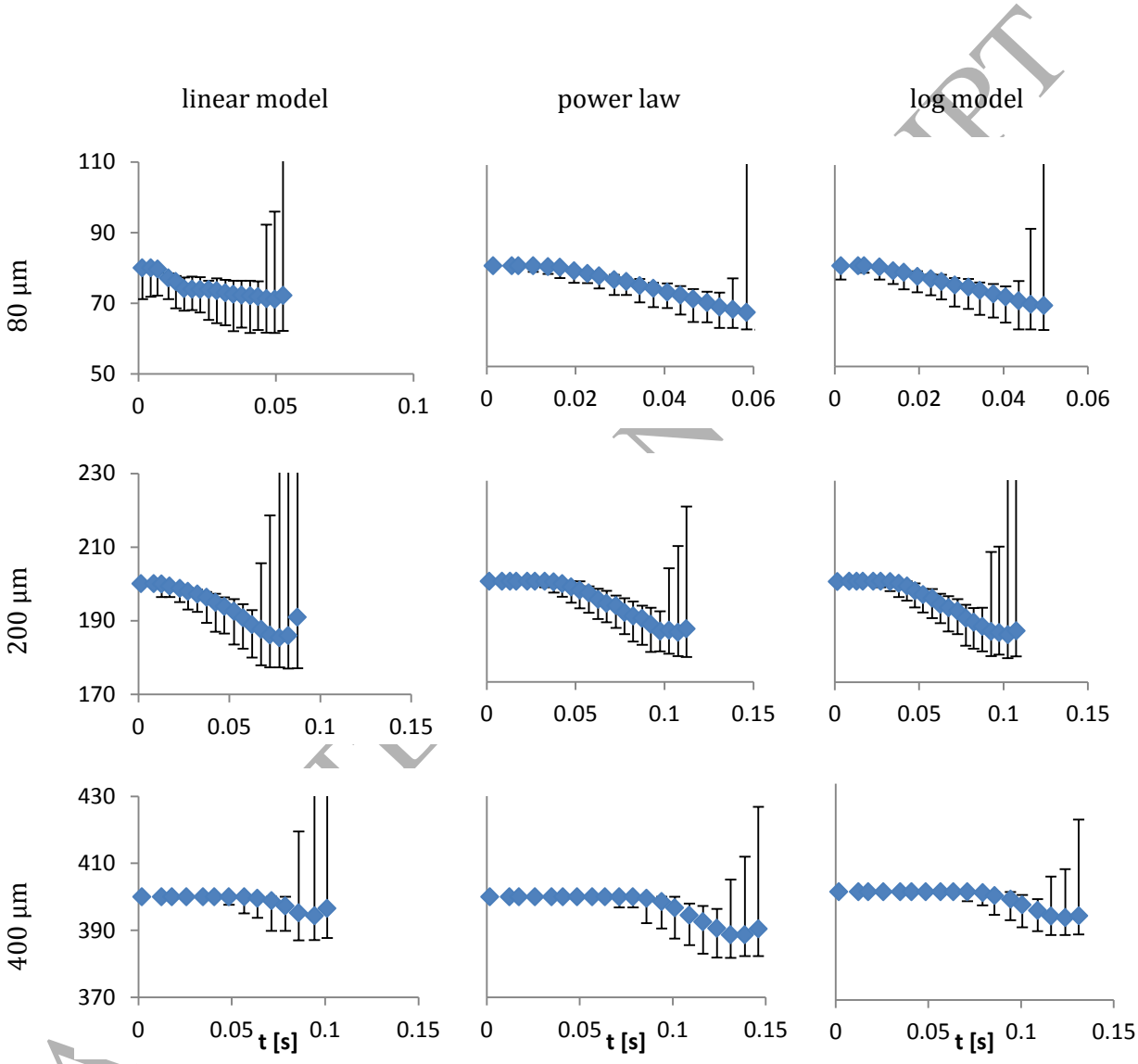

Figure 6: Particle diameter evolution of particles for all swelling models.

overestimates the shrinking effect. As the increasing diameter is of minor interest at this point, the plots were cut to size ranges where the maximum diameter of few particles is out of the plot region, which is clearly marked by the much lower average values.

The shrinking curves already indicate the differences in particle size evolution in the different simulations, which is a consequence of the influence of different gas phase properties on the particles. As the mean diameters of the two larger particle sizes show, the shrinking process is fastest for the linear model, and the mean diameter of the 80 µm particles shows a less continuous temporal evolution for this model compared to the other two models. For comparison, these data was converted into d^2 plots to determine average shrinking rates from mean values. The resulting curves are depicted in Figure 7.

The results show, that the difference between the swelling models has the largest influence on small droplets, which are represented by the 80 µm size fraction. For the three different models

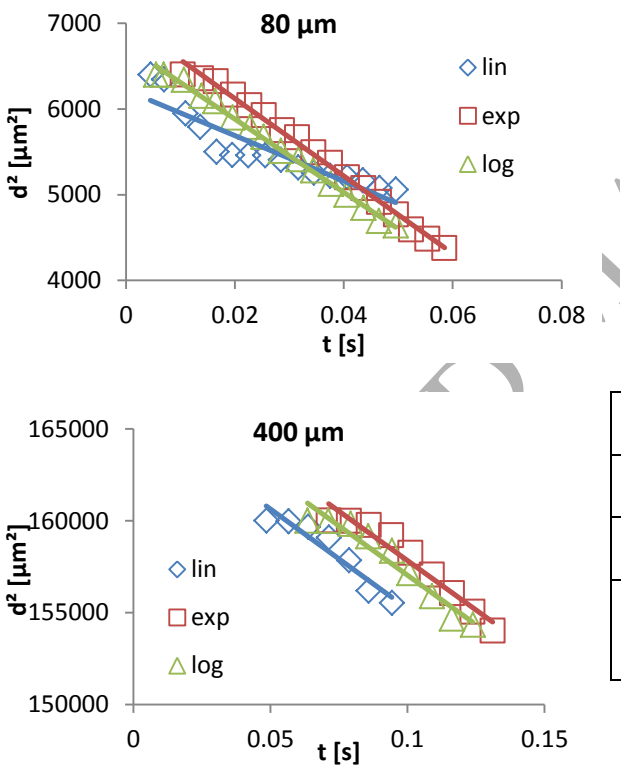

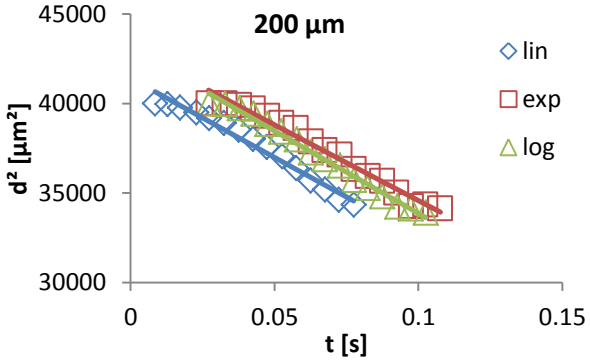

$\tilde{\alpha}$ [10^3 µm²/s]	lin	exp	log
80 µm	26.5	45.2	40.8
200 µm	88.3	84.5	92.2
400 µm	108.1	107.3	107.2

Figure 7: d^2-t plots representing the average shrinking rate $\tilde{\alpha}$ for particle diameters 80, 200 and 400 µm.

shrinking rates between 26.5 and 45.2*10^3µm^{2}s^{-1} were calculated. The d^2 data from 80 µm droplets show that in average the shrinking does not follow a typical d^2 law, for the larger droplet sizes this effect is still visible but less pronounced. Furthermore the results show, that the drop tube experiments in (Schiemann et al., 2012), which led to $\tilde{\alpha}$= 33700 µm^2/s represent a suitable shrinking rate, but the data could be improved by slight variations in shrinking rate.

However measurements with larger (levitated) particles miss the shrinking rates derived from CFD simulations regardless of the swelling model and its effects on the flow field by a factor 4-5.

So far the modelling approach only considers interactions between droplets/particles and the continuous phase. No collisions of the discrete phase, neither for droplets nor particles are included in the modelling approach. The turbulent conditions in many multi-phase systems make droplet or particle collisions relevant (Meyer and Deglon, 2011). Droplet collisions can change the spray propagation, droplet evaporation and distribution, as size and number are changed (Taskiran and Ergeneman, 2014). As causative effects, Qian and Law identified five possible ways of droplet collisions, namely coalescence with minor deformation, bouncing, coalescence after substantial deformation, coalescence followed by separation of near head-on collisions and coalescence followed by separation for off-centre collisions (Qian and Law, 1997). Examples for modelling approaches are the use of population balances (Handscomb et al., 2009) or Lagrangian approaches (Guo et al., 2004). Furthermore particle collisions with walls or other particles could be responsible for particle breakup, and would also have an influence on the flow field, which in turn would affect the chemical conversion.

The linear model applied in this work is based on measurements which represent particle formation conditions similar to those identified in industrial scale reactors. The shrinking rate (or drying history), which is used to determine the onset of swelling in the particle formation model, is underrated by current experimental data for larger particles according to the simulations carried out. Increasing shrinking rates are predicted to lead to earlier shell formation, which would cause larger particle swelling when the stability of the particles is sufficient, but the available information on iron chloride properties does not provide insight into this phenomenon.

Two possible solutions can help to improve the predictive accuracy of numerical modelling of spray roasting reactors:

- Experiments with varying particle sizes and shrinking rates, providing a data base for flexible swelling modelling. A suitable range of drying histories has to be covered.
- Analysis of the initial droplet size distribution and final particle size distribution at given settings of a spray roasting reactor. This would allow determining a general correlation between initial and final size distribution.

6. CONCLUSIONS

Computational fluid dynamics simulations were carried out to investigate the influence of particle swelling models in spray roasting reactors for iron chloride solutions. Based on available experimental data, three empirical models were derived to describe the particle diameter with consideration of particle swelling. A model with linear relation between initial droplet and final particle diameter was compared to two models with logarithmic and power law relation between initial and final diameter. The results show that the flow field, species distribution and particle trajectories are significantly affected by the applied swelling model.

The prediction of initial conditions of the swelling process, in terms of the spatial concentration of iron chloride in the particle, is mainly influenced by the shrinking rate of the particle. It has been shown that the experimental data for small particles cover the relevant range of shrinking rate. For larger particles and the conditions prevailing in spray roasting reactors, as predicted numerically, additional and better corresponding experimental data would help to improve the prediction of reactor performance by use of CFD. The general tendency shows that higher shrinking rates, which were experimentally determined for small droplets, lead to stronger particle swelling. In this case the linear swelling model is the best option as a starting point, but if these large particles lose their mechanical stability, this probably has to be considered to avoid biasing by particle fragmentation.

ACCEPTED MANUSCRIPT

ACCEPTED MANUSCRIPT

References

Abramowitz, M., Stegun, I.A., 1972. Handbook of Mathematical Functions. Dover Publications Inc., New York.

Ansys, I., 2011. ANSYS FLUENT User ' s Guide.

Beck, M., Wirtz, S., Scherer, V., 2007a. Experimental and Numerical Studies of Fe2O3 Particle Formation Processes in a Flat Flame Burner. Chem. Eng. Technol. 30, 790–796. doi:10.1002/ceat.200600393

Beck, M., Wirtz, S., Scherer, V., Bärhold, F., 2007b. Numerical Calculations of Spray Roasting Reactors of the Steel Industry with Special Emphasis on Fe2O3-Particle Formation. Chem. Eng. Technol. 30, 1347–1354. doi:10.1002/ceat.200700231

Brenn, G., 2005. Concentration fields in evaporating droplets. Int. J. Heat Mass Transf. 48, 395–402. doi:10.1016/j.ijheatmasstransfer.2004.07.039

Brenn, G., 2004. Concentration Fields in Drying Droplets. Chem. Eng. Technol. 27, 1252–1258. doi:10.1002/ceat.200407025

Ferreira, A.S., Mansur, M.B., 2011. Statistical analysis of the spray roasting operation for the production of high quality Fe2O3 from steel pickling liquors. Process Saf. Environ. Prot. 89, 172–178. doi:10.1016/j.psep.2010.11.005

Guo, B., Fletcher, D.F., Langrish, T.A.G., 2004. Simulation of the agglomeration in a spray using Lagrangian particle tracking. Appl. Math. Model. 28, 273–290. doi:10.1016/S0307-904X(03)00133-1

Handscomb, C.S., Kraft, M., Bayly, A.E., 2009. A new model for the drying of droplets containing suspended solids. Chem. Eng. Sci. 64, 628–637. doi:10.1016/j.ces.2008.04.051

Jedlicka, H., 1978. Spray Roasting regeneration of spent HCl as applied to small pickling plants. Iron Steel Eng. Int. Technol. world Compet. 55, 73–75.

Johansson, S., Geza, V., Westerberg, L.G., Jakovics, A., 2010. Characteristics of flow and temperature distribution in a Ruthner process, in: 6th International Scientific Colloquium: Modelling for Material Processing. University of Latvia, Riga, pp. 317–322.

Johansson, S., Westerberg, L.G., Lundstr, T.S., 2014. Gas and Particle Flow in a Spray Roaster. J. Appl. Fluid Mech. 7, 187–196.

Kladnig, W.F., 2003. A review of steel pickling and acid regeneration an environmental contribution. Int. J. Mater. Prod. Technol. 19, 550. doi:10.1504/IJMPT.2003.003471

Menter, F.R., 1994. Two-equation eddy-viscosity turbulence models for engineering applications. AIAA J. 32, 1598–1605. doi:10.2514/3.12149

Meyer, C.J., Deglon, D.A., 2011. Particle collision modeling - A review. Miner. Eng. 24, 719–730. doi:10.1016/j.mineng.2011.03.015

Peek, E.M.L., 1996. Chloride Pyrohydrolysis, lixiviant regeneration and metal separation. Delft.

Qian, J., Law, C.K., 1997. Regimes of coalescence and separation in droplet collision. J. Fluid Mech. 331, 59–80. doi:10.1017/S0022112096003722

Raithby, G.D., Chui, E.H., 1990. A Finite-Volume Method for Predicting a Radiant Heat Transfer in Enclosures with Participating Media. J. Heat Transf. 112, 415–423.

Schiemann, M., 2011. Pyrohydrolyse eisenchloridhaltiger Lösungen in Sprühröstreaktoren. Ruhr-Universität Bochum.

Schiemann, M., Baer, S., Esen, C., Ostendorf, A., 2015. Drying of Iron Chloride Solutions: Laser Heating of Levitated Single Particles. Chem. Eng. Technol. 38, 947–951. doi:10.1002/ceat.201400594

Schiemann, M., Wirtz, S., Scherer, V., Bärhold, F., 2013. Spray Roasting of Iron Chloride FeCl2: Numerical Modelling of Industrial Scale Reactors. Powder Technol. 245, 70–79. doi:10.1016/j.powtec.2013.04.034

Schiemann, M., Wirtz, S., Scherer, V., Bärhold, F., 2012. Spray roasting of iron chloride FeCl2: laboratory scale experiments and a model for numerical simulation. Powder Technol. 228, 301–308. doi:10.1016/j.powtec.2012.05.037

Smith, T.F., Shen, Z.F., Friedman, J.N., 1982. Evaluation of Coefficients for the Weighted Sum of Gray Gases Model. J. Heat Transfer 104, 602–608. doi:10.1115/1.3245174

Taskiran, O.O., Ergeneman, M., 2014. Trajectory based droplet collision model for spray modeling. Fuel 115, 896–900. doi:10.1016/j.fuel.2012.11.053

Westerberg, L.G., Geza, V., Jakovics, A., Lundström, T.S., 2011. Burner Backflow Reduction in Regeneration Furnace. Eng. Appl. Comput. Fluid Mech. 5, 372–383. doi:10.1080/19942060.2011.11015379

Wilke, C.R., Chang, P., 1955. Correlation of diffusion coefficients in dilute solutions. AICHE J. 1, 264–270.

Table 1: Burner feed parameters, composition given in [kg/kg$_{total}$]

$\dot{m}$ [kg/s]	0.6
T [K]	1085
CH_4	0.0184
O_2	0.1612
CO_2	0.050
H_2O	0.040

Table 2: Cl- and FeO content of particle samples at the particle outlet in percent per weight.

	linear law	power law	ln law
Cl [w%]	0.008	0.53	0.26
FeO [w%]	0.015	0.006	0.16
t [s]	65.0	25.2	40.9

ACCEPTED MANUSCRIPT